Analysis of Intercalation/De-Intercalation of Li Ions Into/From Graphite at 0 °C via Operando Synchrotron X-ray Diffraction

Journal of The Electrochemical Society, 2021 **168** 090515

Analysis of Intercalation/De-Intercalation of Li Ions Into/From Graphite at 0 °C via Operando Synchrotron X-ray Diffraction

Hiroyuki Fujimoto,[1,z] Shigeharu Takagi,[1] Keiji Shimoda,[1] Hisao Kiuchi,[1] Kenichi Okazaki,[1] Tetsuyuki Murata,[1] Zempachi Ogumi,[1,*] and Takeshi Abe[2,]**

[1]*Office of Society-Academia Collaboration for Innovation, Kyoto University, Kyoto 611-0011, Japan*
[2]*Graduate School of Global Environmental Studies, Kyoto University, Kyoto 615-8510, Japan*

The charge/discharge reaction mechanisms of graphite negative electrodes in Li ion batteries were investigated via operando synchrotron X-ray diffraction at 0 °C and 25 °C. The intercalation of Li ions at 25 °C formed the stage 1 compound with an in-plane structure of LiC_6; while intercalation at 0 °C only formed stage 2, with in-plane structures of LiC_9 and LiC_6. The degree of graphite expansion in the *a, b*-axes and *c*-axis directions by intercalation at 0 °C was less than that at 25 °C. Hence, it was difficult to form the stage 1 structure by further increases in the Li ion concentration, and the charging reaction at low temperature became difficult. De-intercalation at 0 °C did not follow the Daumas–Hérold model and proceeded discretely in the order: stage 1 → stage 2 → stage 4 → graphite, without going through stages 3, 5–8 and dilute stage 1.

 [DOI: 10.1149/1945-7111/ac2280]

Manuscript submitted July 27, 2021; revised manuscript received August 20, 2021. Published September 8, 2021.

Lithium ion batteries (LIBs) have expanded applications from information technology devices and portable audio-visual devices to electric vehicles (EV) and energy storage since the first commercialization by Sony Corporation. It is an essential device in today's information-technology-based societies. Increased market expansion requires higher performances and further cost reductions. There have been many studies concerning the negative electrode materials in LIBs. However, most commercial LIBs still use graphite. To improve the LIB energy density, durability, and safety, it is essential to develop new materials and to elucidate the detailed reaction mechanisms. In particular, EV batteries are required to have high charge/discharge rates without impairing safety. In EV batteries, the deposition of metallic Li on the negative electrode must be suppressed during high-rate charging at low temperatures. Low output power when starting in cold weather is also a major issue. These charge/discharge rate problems are due to the poor performance of the graphite negative electrode at low temperature. The fundamental reaction mechanism of the negative electrode involves the formation of stage 1 li-graphite intercalation compound (Li-GIC) with a LiC_6 structure; the theoretical capacity of that composition is 372 $Ahkg^{-1}$. Li intercalation (charge) and de-intercalation (discharge) into/from the graphite are separated into several elementary steps involving ionic conduction in the electrolyte phase, interfacial Li^+ transfer,[1,2] Li^+ transfer within particulates of active materials, and phase transitions of the materials.[3,4] Li^+ transfer into the graphite interlayers and the phase transitions are not thoroughly understood, while each step directly affects the negative electrode performance. This leads to serious concerns of battery safety.

Many reports have addressed the structure and physical properties of Li-GICs since the first report by Hérold.[5] Stage 1 and stage 2 compounds both have the same in-plane structure defined by p$(\sqrt{3}\times\sqrt{3})$R30°, as shown in structure E[5–10] of Fig. 1. The former has a space group P6/mmm with $a_0 = 0.4305$ nm and $c_0 = 0.3706$ nm, and the latter has a space group P6/mmm with $a_0 = 0.4288$ nm and $c_0 = 0.7063$ nm. In addition, Billaud et al. prepared several Li-GICs at different stages and indexed 00 *l* diffractions for stages 1–5. They found another stage 2 compound (LiC_{18}) with a LiC_9 type in-plane structure of p(3 × 3)R0° (shown in Fig. 1, structure D),[11,12] However, the structures of higher stage compounds (⩾ Stage 3) have not been clarified, and the details of the charge/discharge mechanisms of Li-ion batteries remain unclear. Recent reports, based on ^{7}Li-NMR, proposed LiC_{9n} structures for the higher stages.[13,14] Elucidation of the dynamic behavior of Li-GIC stage formation is very important for improving the graphite negative electrode performance in LIBs.

Recently, *operando* synchrotron X-ray diffraction (SXD) was performed during charge/discharge processes of the LIB graphite electrode, including a detailed analysis of Bragg *d* values for the 002, 101, and 100 graphite diffractions.[15] Several inflections appeared in the *d*-value plot as a function of *x* for LiC_x when *x* was close to a multiple of 6, 9, and 72. Furthermore, these inflections also appeared at the same compositions on the charge/discharge curves and corresponding differential curves (*V*-d*Q*d*V*). A new in-plane superlattice of LiC_{72n} ($n = 1, 2$) was proposed in addition to LiC_{6n} ($n = 1, 2$) and LiC_{9n} ($n = 3$–8). The relationship between the stage structures and the in-plane superlattices is shown in Fig. 1. In addition, we clarified that, when Li ions intercalate, the in-plane structure change firstly occurs along the *a*, *b*-axes direction in order to stabilize and uniform the conjugated π electron system disturbed by the charge transfer of electrons between the graphene and Li ion in conjunction with the stage structural change along the *c*-axis. However, in the charge/discharge reactions at high rates or at a low temperature, the 372 $Ahkg^{-1}$ discharge capacity based on LiC_6 could not be obtained. This implied that the reaction pathway differed from that at room temperature. Here, the work focused on the SXD analysis of stage and in-plane structural changes induced by Li intercalation/de-intercalation at low temperatures. The results will enable engineers to enhance the rate performance of LIB graphite negative electrodes.

In this paper, in order to distinguish between LiC_6 type and LiC_9 type Stage 2 compounds, they are referred to as Stage 2_6 ($LiC_{6\times2}$) and Stage 2_9 ($LiC_{9\times2}$), respectively.

Experimental

The operando SXD analysis of the graphite negative electrode used an aluminum laminate cell (electrode area of 20 mm × 20 mm) shown in Fig. 2, as previously reported.[15] Natural graphite (OMAC-R from Osaka Gas Chemical Co., Ltd., Japan), metallic Li, and 1M-$LiPF_6$/ ethylene carbonate + ethyl methyl carbonate (3:7) were used as the working electrode, counter electrode, and cell electrolyte solution, respectively. After charging and discharging the cell for one cycle in advance, the operando measurement during the charge (intercalation) process was performed during the second cycle at a 0.1 CA current rate at 0 °C and 25 °C in a potential range of

*Electrochemical Society Fellow.
**Electrochemical Society Member.
[z]E-mail: fujimoto.hiroyuki.5n@kyoto-u.ac.jp

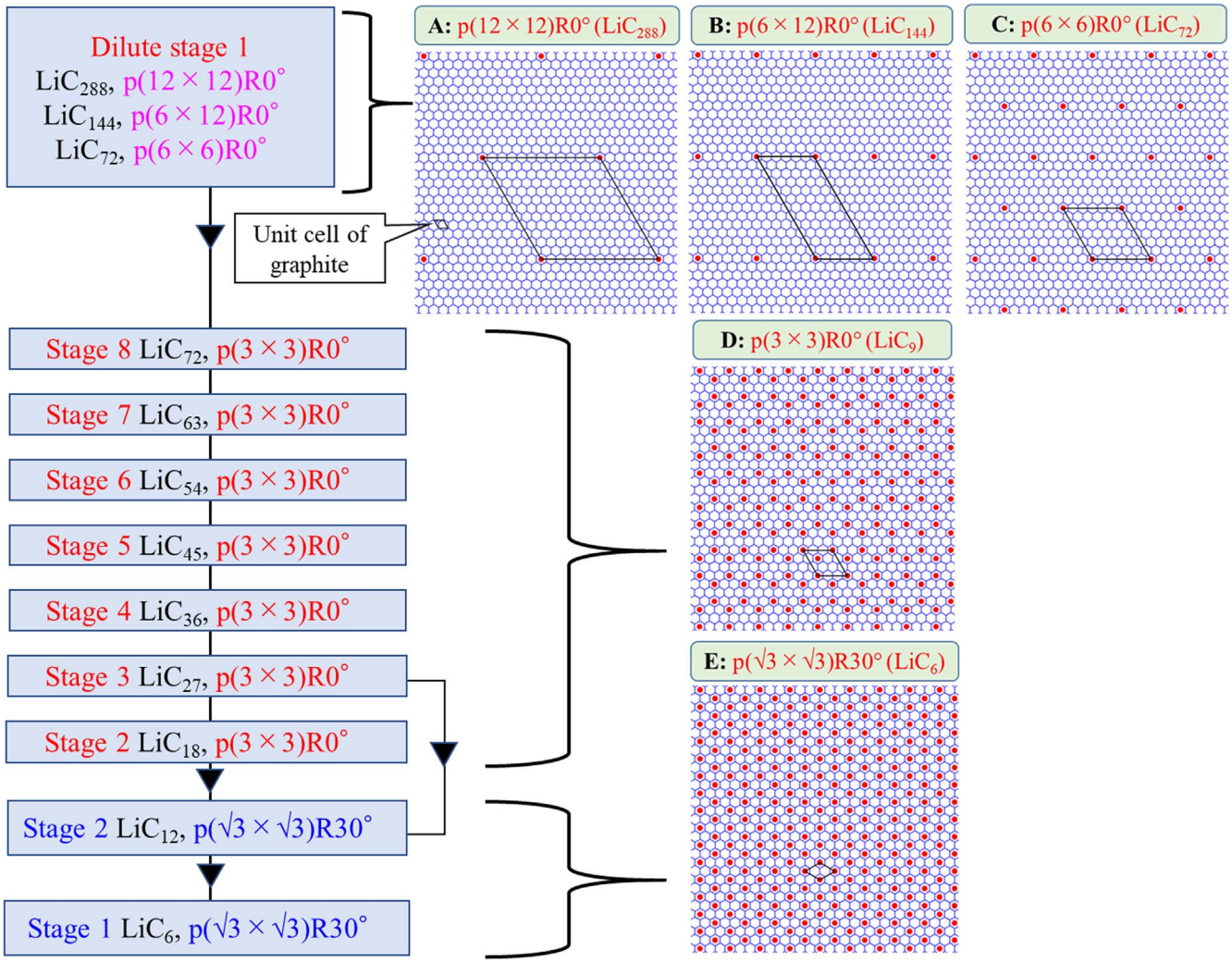

Figure 1. Schematic of Li-GIC structure changes. In the notation used for the in-plane superlattices, p denotes a primitive unit cell, ($i \times j$) denotes the unit vectors measured in units of $a_0 = 0.24612$ nm in the hexagonal lattice primitive cell in Fig. 1A, and Rθ denotes the angle of rotation of the unit vectors of the superlattice relative to the graphite unit vectors.

2.5–0.01 V. The operando measurements during discharge (de-intercalation) at 0 °C were performed after charging at 25 °C, followed by cooling to 0 °C, because the fully charged compound with a saturated composition of LiC_6 could not be obtained during charging at 0 °C. The SXD measurements were performed repeatedly using the SPring-8 BL28XU beamline (wavelength of 0.049592 nm (25 keV), and beam area of 0.2 mm × 0.5 mm) with 10 sec exposure times. The diffraction profiles were acquired by the transmission method.

About 3600 continuous profile datasets were obtained at the 0.1 CA rate during intercalation/de-intercalation. The analyses were performed while synchronizing the datasets with the charge/discharge curves, their differential curves (V-dQ/dV), and the LiC_x composition. The operando analysis software "Profile Chaser" was used, as reported previously.[15]

Results and Discussion

Intercalation at 0 °C.—Figure 3A shows the charge curves of the 0.1 CA current rate at 0 °C and 25 °C. At 0 °C, the capacity (253 Ahkg^{-1}) was significantly lower than that at 25 °C. In particular, the potential plateau regions corresponding to the formation of stage 2 and stage 1 at 0 °C were smaller than those at 25 °C. Also, the inflection points in the LiC_{108}, LiC_{72}, LiC_{27}, and LiC_{12} compositions at 25 °C were slightly deviated at 0 °C. The V-dQ/dV curves in Fig. 3B contained five reduction peaks at both 0 °C and 25 °C. Basically, it appeared that the same reaction was occurring at both temperatures, but the peak I intensity at 0 °C was relatively weaker than that at 25 °C. This peak corresponded to the transition from stage 2 to stage 1. The stage 1 plateau region in the charge curve at 0 °C was also smaller than that at 25 °C. Hence, there could have been an inhibition in the formation of stage 1.

Figure 4 shows the dynamic changes in the 100 and 002 diffraction profiles of graphite during charging at every 1% state of charge (SOC) at 0 °C and 25 °C. The largest difference between the two was that no stage 1 formation was observed in the 100 or 002 diffraction profiles at 0 °C. Considering that stage 1 formation started around $LiC_{9.5}$ at 25 °C, the domain size of stage 1 at 0 °C might not have been large enough for detectable diffractions. In addition, the formation region of stage 2 ($LiC_{15.5}$–$LiC_{8.9}$) was considerably narrower than that at 25 °C (LiC_{21}–$LiC_{6.5}$). The results are in good agreement with the charge curve profile.

Figure 5A plots d_{100} and d_{002} values as a function of x in $LiCx$. Increases in d_{100} and d_{002} values with increased Li concentration at 0 °C were smaller than those at 25 °C. The C=C bond length, $d_{C=C}$, in the six-membered graphite carbon ring is geometrically related to d_{100} by:

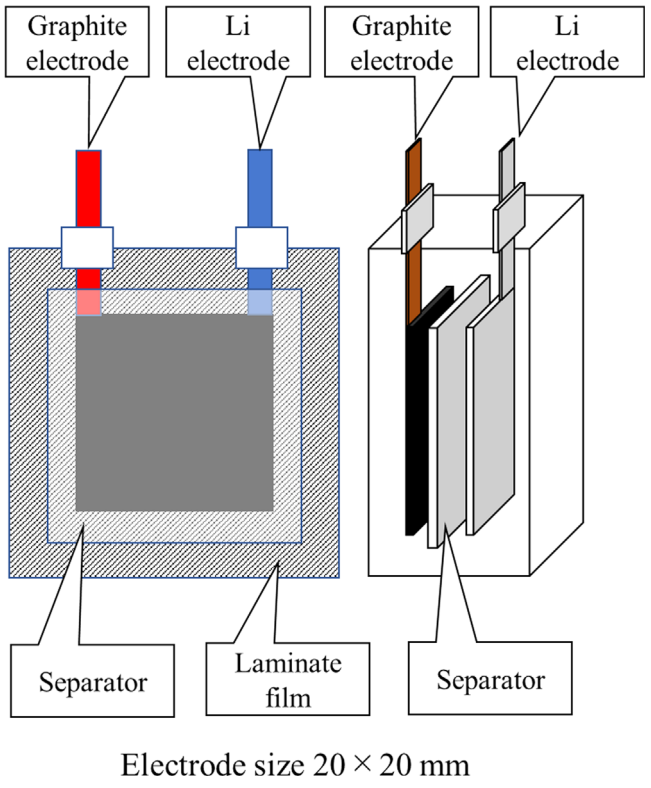

Figure 2. Schematic of the cells for operando X-ray diffraction.

expansion coefficient is negative below 400 °C. Hence, thermal shrinkage occurs more easily at 0 °C, and thermal vibrations of the carbon atoms mainly occur along the *c*-axis direction. However, the thermal expansion coefficient along the *c*-axis direction also decreases at lower temperatures.[18–20] Hence, the expansion along the *c*-axis by insertion of Li ions and the formation of the nested structure would be more difficult at 0 °C than at 25 °C. Due to these factors, the intercalation reaction proceeds only to the stage 2 structure; it cannot proceed without further expansion of the six-membered ring size and expansion in the *c*-axis direction. Therefore, low-temperature charging (intercalation) becomes difficult. To verify this behavior in more detail, the diffraction profiles for LiC_9, LiC_{12}, and LiC_{18} in Fig. 4 were fit in Fig. 6. At 25 °C, the two peaks for LiC_{18} that could be attributed to stage 3_9 and stage 2_6 were observed for both *hk*0 and 00 *l* diffractions, indicating a mixed stage compound. For LiC_{12}, both *hk*0 and 00 *l* diffractions showed a single peak, and this compound is almost the pure stage 2_6. In LiC_9, a mixture of stage 2_6 and stage 1_6 was formed. At 0 °C, LiC_{18} showed almost a single peak assigned to stage 2_9, and the LiC_{12} was a mixture of stage 2_9 and stage 1_6. In LiC_9, only stage 2_6 was observed. These results showed that, at 0 °C, stage formation was delayed relative to that at 25 °C. As mentioned above, the thermal expansion coefficient along the *c*-axis and the thermal vibrational effect of the C=C bonds decrease at low temperatures. Thus, the expansion of the six-membered ring and the expansion along the *c*-axis are less likely to occur. This clearly shows that the intercalation reaction was hindered and that the charge reaction at low temperature was suppressed.

De-intercalation at 0 °C.—Because the cell could not be fully charged at 0 °C, it was fully charged in advance at 25 °C, followed

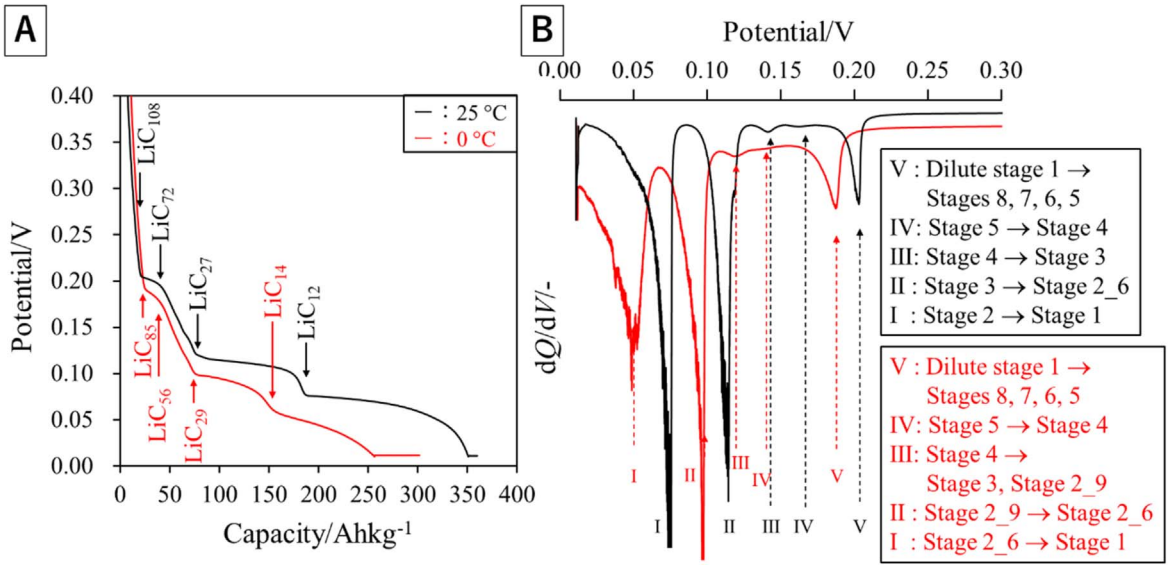

Figure 3. Charge curves and their differential curves (*V*-d*Q*/d*V*) at 0 °C and 25 °C.

$$d_{C=C} = 2/3d_{100}.$$

Thus, $d_{C=C}$ increases with d_{100}. This indicates that the six-membered ring expands as the Li ion concentration increases, and that the degree of expansion at 0 °C was smaller than that at 25 °C. When the Li ions intercalate, they must first spread between adjacent graphene sheet layers. Then, the six-membered carbon ring expands to form a nested structure in which part of the Li ion is buried in the center of the ring. This delocalizes and stabilizes the conjugated graphene π-electron system via charge transfer between the graphene sheet and Li.[16,17] The C=C bond in the ring is extremely strong and its

by cooling to 0 °C. Then, it was discharged (de-intercalated) at 0 °C. Figure 7 shows the discharge curves at 0 °C and 25 °C. Although the discharge capacities were almost the same at 0 °C and 25 °C, the positions of the inflection points were different, as seen in the case of charging. This indicated that the de-intercalation mechanism at 0 °C was different from that at 25 °C. Similar to the charging results, there was a significant difference in the potential plateau region that corresponded to de-intercalation of Li ions from stage 1 and stage 2. In the *V*-d*Q*/d*V* curve, five peaks associated with stage transitions were observed at 25 °C, but only three peaks were observed at 0 °C. This indicated a clear difference in the stage transition behavior between 0 °C and 25 °C.

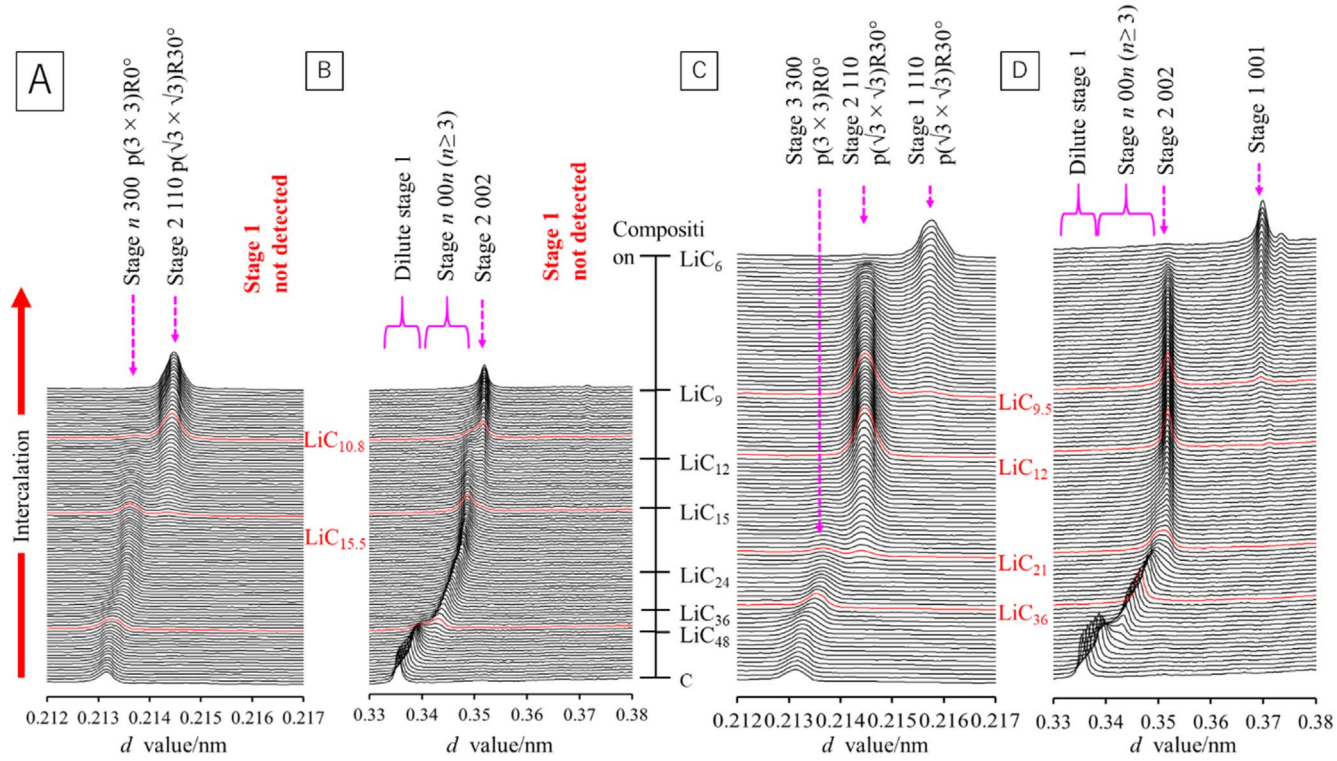

Figure 4. Dynamic changes in the 100 and 002 diffractions of graphite during intercalation at 0 °C (A), (B) and 25 °C (C), (D).

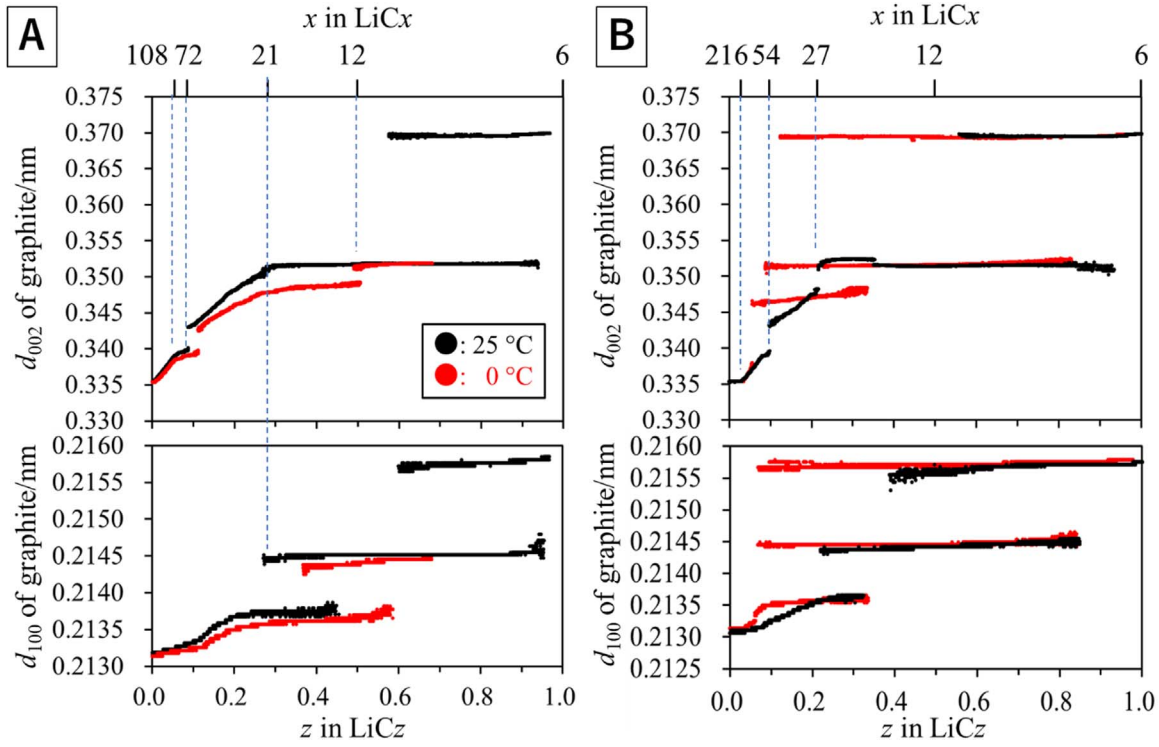

Figure 5. Dynamic changes of d_{100} and d_{002} values of graphite as a function of x in LiC_x.

Figure 8 shows the changes in the SXD profile during discharging at every 1% SOC at 0 °C and 25 °C. In addition, Fig. 5B shows the composition dependence of the d_{100} and d_{002} values. In Figs. 8B, 8D, the stage changes are completely different for the dynamic changes in the c-axis direction at 0 °C and 25 °C. At 25 °C, the diffraction position shifted continuously from $d = 0.351$ nm (stage 2) to $d = 0.3354$ nm (002 of graphite) via dilute stage 1. However, at 0 °C, the 00 l diffraction positions located discretely at $d = 0.370$ nm (stage 1), 0.351 nm (stage 2), 0.345 nm (stage 4), and 0.3354 nm (002 of graphite). Similarly, hk0 diffractions loated discretely at $d =$ 0.2157 nm (110 of stage 1_6), 0.2144 nm (110 of stage 2_6), 0.2135 nm (300 of stage 4_9), and 0.2131 nm (100 of graphite).

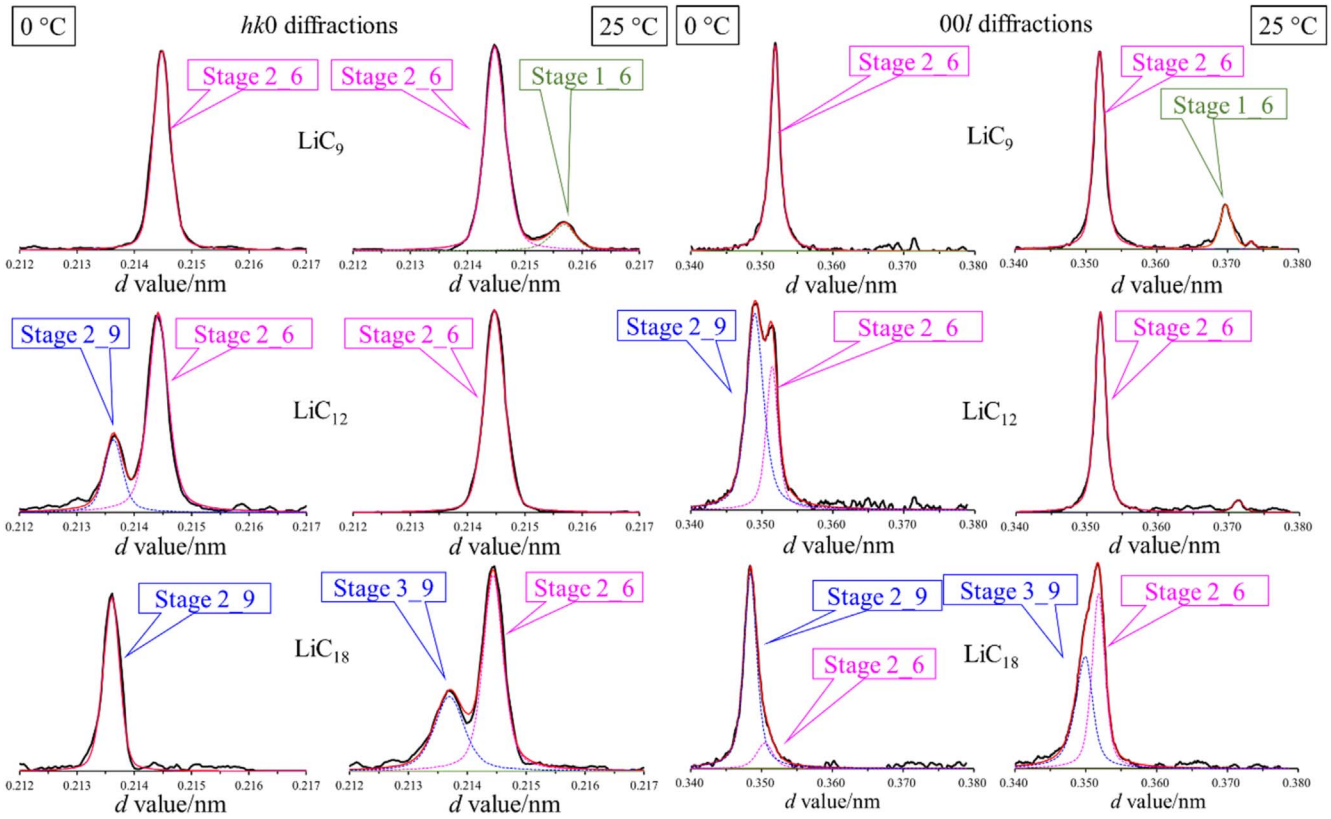

Figure 6. Profile fitting of *hk*0 and 00 *l* diffractions of Li-GIC with the compositions of LiC_9, LiC_{12}, LiC_{18}.

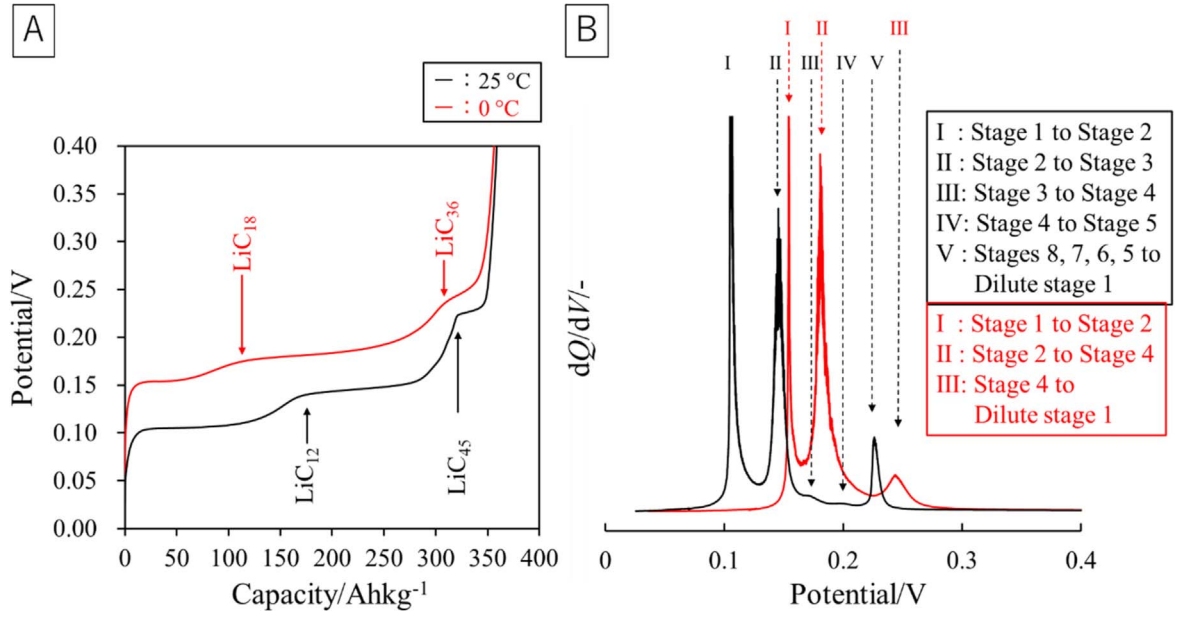

Figure 7. Discharge curves and their differential curves (V-dQ/dV) at 0 °C and 25 °C.

Regarding the continuous peak shifts at 25 °C, we reported previously that the change in the diffraction (stage change) proceeds in the order stage 1 → stage 2 → stage 2 L → stage 3 → stage 4 → stages 5,6,7,8 → dilute stage 1 → graphite. However, at 0 °C, the de-intercalation proceeded discretely in the order stage 1 → stage 2 → stage 4 → graphite without going through stage 2 L, stage 3, and stages 5–8. This behavior suggests that de-intercalation does not follow the Daumas–Hérold model at low temperatures.[21]

Conclusions

At 0 °C, the thermal expansion coefficient along the *c*-axis direction and the thermal vibrational effect of the C=C bonds decrease. Therefore, expansion of the six-membered ring and that along the *c*-axis direction were less likely to occur. Hence, Li intercalation formed the stage 2_6 structure, and formation of the stage 1_6 structure was inhibited. Because the intercalation led to LiC_9, the charging reaction hardly occurred. As mentioned in the

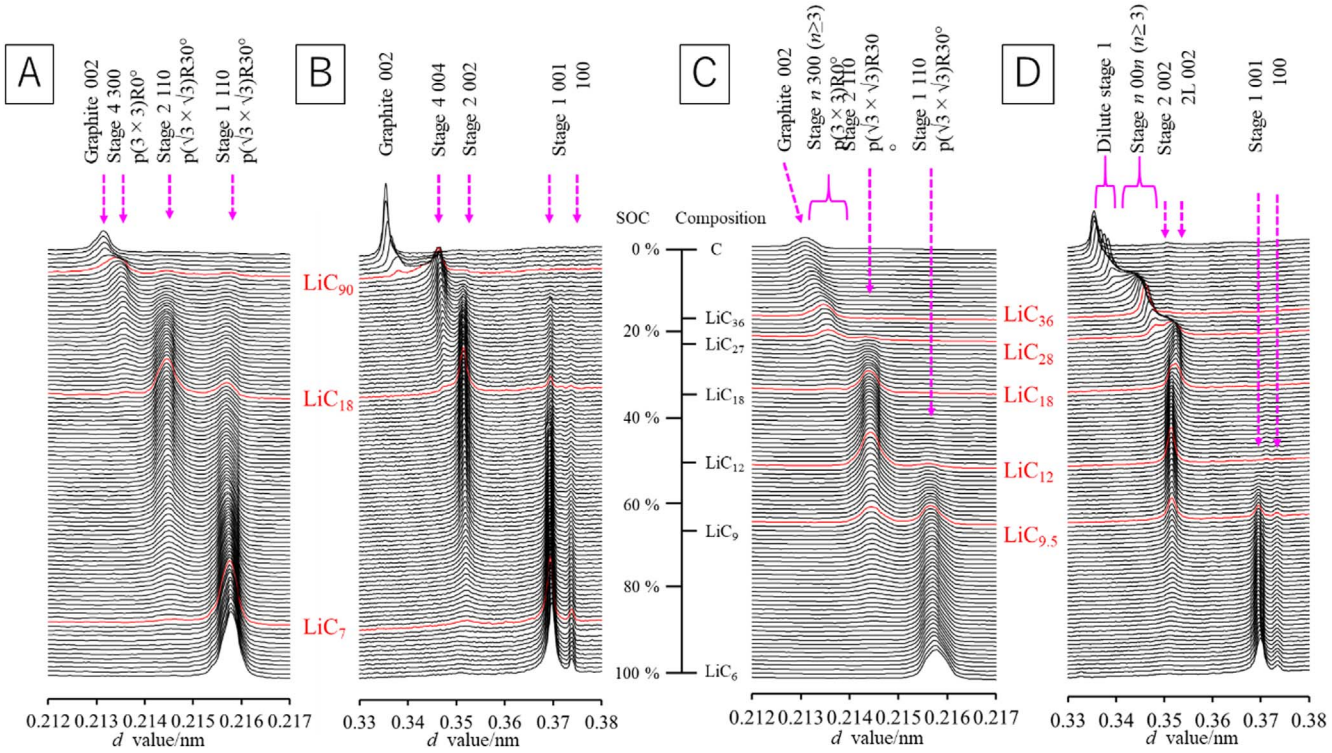

Figure 8. Dynamic changes of 100 and 002 diffractions of graphite during deintercalation. at 0 °C (A), (B) and 25 °C (C), (D).

introduction, the charging reaction can be divided into several elementary steps. That is, (1) ion conduction in the electrolyte, (2) transfer of Li ions at the electrode interface, (3) transfer of Li ions into the active material particles, and a phase transition of graphite. In this paper, we could examine only for the third item in detail in these steps, but the contribution of items (1) and (2) to the reaction at low temperatures can not be discussed only from these dataset. Furthermore, de-intercalation did not follow the Daumas–Hérold model and proceeded discretely in the order stage 1 → stage 2 → stage 4 → graphite, without the formation of several stages.

Acknowledgments

This work was supported by the Research and Development Initiative for Scientific Innovation of New Generation Batteries 2 (RISING2) project and the New Energy and Industrial Technology Development Organization (NEDO). The synchrotron X-ray diffraction experiments were performed on the BL28XU beamline at the SPring-8 facility with the approval of the Japan Synchrotron Radiation Research Institute (JASRI) (proposal nos. 2016A7602, 2016B7603, 2017A7603, 2017B7603, 2018A7603, 2019A7613 and 2019B7613). We thank Alan Burns from the Edanz Group (https://jp.edanz.com/ac) for editing a draft of this manuscript.

Data availability statement

N.A

ORCID

Hiroyuki Fujimoto https://orcid.org/0000-0003-4562-7715
Ken-ichi Okazaki https://orcid.org/0000-0003-0800-712X

References

1. Z. Ogumi, T. Abe, T. Fukutsuka, S. Yamate, and Y. Iriyama, *J. Power Sources*, **127**, 72 (2004).
2. T. Doi, K. Miyatake, Y. Iriyama, T. Abe, and Z. Ogumi, *Carbon*, **42**, 3183 (2004).
3. A. Funabiki, M. Inaba, T. Abe, and Z. Ogumi, *J. Electrochem. Soc.*, **146**, 2443 (1999).
4. A. Funabiki, M. Inaba, T. Abe, and Z. Ogumi, *Electrochim. Acta*, **45**, 865 (1999).
5. A. Hérold, *Bull. Soc. Chim. France*, **187**, 999 (1955).
6. D. Guerard and A. Hérold, *Carbon*, **13**, 337 (1975).
7. N. Kambe, M. S. Dresselhaus, G. Dresselhaus, S. Basu, A. R. McGhie, and J. E. Fischer, *Mat. Sci. Eng.*, **40**, 1 (1979).
8. D. Gerard, M. Chaabouni, P. Lagrange, M. E. Makrini, and A. Hérold, *Carbon*, **18**, 257 (1980).
9. M. S. Dresselhaus and G. Dresselhaus, *Adv. Phys.*, **30**, 139 (1981).
10. N. Emery, C. Hérold, and P. Lagrange, *Prog. Solid State Chem.*, **36**, 213 (2008).
11. D. Billaud, E. McRae, J. F. Mareche, and A. Hérold, *Synth. Met.*, **3**, 21 (1981).
12. S. B. Dicenzo, S. Basu, and G. K. Werthem, *Synth. Met.*, **3**, 139 (1981).
13. M. Letellier, F. Chevallier, and M. Morcrette, *Carbon*, **45**, 1025 (2007).
14. F. Chevallier, F. Poli, B. Montigny, and M. Letellier, *Carbon*, **61**, 140 (2013).
15. H. Fujimoto, H. Kiuchi, S. Takagi, K. Shimoda, K. Okazaki, Z. Ogumi, and T. Abe, *J. Electrochem. Soc.*, **168**, 040509 (2021).
16. F. Okino and N. Bartlett, *J. Chem. Soc., Dalton Trans.*, 2081 (1993).
17. F. Okino, *Tanso*, **145**, 277 (1990).
18. B. T. Kelly and P. L. Walker, *Carbon*, **8**, 211 (1970).
19. B. T. Kelly, *Carbon*, **10**, 429 (1972).
20. B. T. Kelly, *Carbon*, **11**, 379 (1973).
21. N. Daumas and A. Hérold, *C. R. Acad. Sci. Ser. C*, **268**, 373 (1969).